Nat Hazards (2012) 64:1491–1510
DOI 10.1007/s11069-012-0311-5

ORIGINAL PAPER

Estimating tsunami potential of earthquakes in the Sumatra–Andaman region based on broadband seismograms in India

S. K. Singh · J. F. Pacheco · M. Ordaz · R. S. Dattatrayam · G. Suresh · P. R. Baidya

Received: 7 November 2011 / Accepted: 19 July 2012 / Published online: 29 July 2012

Abstract In this paper, we report that the ratio of broadband energy (0.01–2 Hz) to high-frequency energy (0.3–2 Hz), E_r, estimated from regional seismograms of India, might be a useful parameter in estimating tsunami potential of earthquakes in the Sumatra–Andaman region. E_r is expected to be sensitive to the depth as well as to the source characteristics of an earthquake. Since a shallow and slow earthquake has a greater tsunamigenic potential, E_r may be a useful diagnostic parameter. We base our analysis on broadband seismograms of the great earthquakes of Sumatra–Andaman (2004, $M_w \sim 9.2$) and Nias (2005, M_w 8.6), 41 of their aftershocks, and the earthquakes of north Sumatra (2010, M_w 7.8) and Nicobar (2010, M_w 7.4) recorded at VISK, a station located on the east coast of India. In the analysis, we also included the two recent, great strike-slip earthquakes of north Sumatra (2012, M_w 8.6, 8.2) recorded at VISK and three south Sumatra earthquakes (2007, M_w 8.5; 2007, M_w 7.9; 2010, M_w 7.8) recorded at PALK, a station in Sri Lanka. We find that E_r is a function of depth; shallower earthquakes have higher E_r values than the deeper ones. Thus, E_r may be indicative of tsunamigenic potential of an earthquake. As M_w and E_r increase so does the tsunami potential. In addition to the parameter E_r, the radiated seismic energy, E_s, may be estimated from the regional seismograms in India using empirical Green's function technique. The technique yields reliable E_s for the great Sumatra and Nias earthquakes. E_r and E_s computed from VISK data, along with M_w and focal mechanism, may be useful in

S. K. Singh
Instituto de Geofísica, Universidad Nacional Autónoma de México, Ciudad Universitaria, 04510 Mexico, DF, Mexico

J. F. Pacheco (✉)
Observatorio Vulcanológico y Sismológico de Costa Rica, Universidad Nacional, 40101 Heredia, Costa Rica
e-mail: jpacheco@una.ac.cr

M. Ordaz
Instituto de Ingeniería, Universidad Nacional Autónoma de México, Ciudad Universitaria, 04510 Mexico, DF, Mexico

R. S. Dattatrayam · G. Suresh · P. R. Baidya
India Meteorological Department, Lodhi Road, New Delhi 110003, India

estimating tsunami potential along the east coast of India from earthquakes in the Sumatra–Andaman region in less than ~20 min.

Keywords Early tsunami warning · Indian Ocean tsunami · 2004 Sumatra earthquake · Radiated energy of Sumatra and Nias earthquakes

1 Introduction

Tsunamis produced by recent great earthquakes of Sumatra–Andaman (December 26, 2004, M_w 9.2) and Tohoku-oki (2011, M_w 9.1) resulted in unprecedented death and destruction. The tsunami caused by the Sumatra–Andaman earthquake claimed more than 280,000 lives in Indonesia, Thailand, Sri Lanka, and India and left about 1.5 million homeless. To prevent future loss of lives, early tsunami warning systems have been developed and deployed in the region. In particular, India has implemented its own warning system. National Tsunami Early Warning System (NTEWS) has been established at the Indian National Centre for Ocean Information Services (INCOIS), Hyderabad. As part of the effort, a 17-station Real Time Seismic Monitoring Network (RTSMN) has been set up by the India Meteorological Department (IMD) (Dattatrayam et al. 2009). RTSMN and IRIS data are now being routinely used by IMD to determine location and magnitude of earthquakes in the region and to flag those with potential for tsunami (Dattatrayam et al. 2009).

Early tsunami warning systems mostly rely on magnitude and location of an earthquake. A large magnitude earthquake with a location near the trench of a subduction zone is potentially a tsunamigenic event. Appropriate magnitudes for tsunami warning are those that are based on long-period seismic waves (Abe 1979), for example, the moment magnitude, M_w (Kanamori 1977), or the mantle-wave magnitude, M_M (Brune and Engen 1969; Talandier and Okal 1989). Lockwood and Kanamori (2006) showed that *W*-phase (the long-period wave that arrives between P and S waves) could be retrieved from wavelet analysis that may be useful in quick identification of great earthquakes and high tsunami potential. Presently, *W*-phase is being routinely used to invert for centroid moment tensor (Kanamori and Rivera 2008; Hayes et al. 2009). This solution is extremely useful for early tsunami alert since it can be determined in a relatively short time. Real-time analysis of near-source GPS data seems very promising in quick estimation of critical source parameters, including M_w (e.g., Singh et al. 2012).

An earthquake that generates disproportionately large tsunami in relation to its surface-wave magnitude, M_s, is denoted as a tsunami earthquake (Kanamori 1972). Mechanisms proposed for such earthquakes include slip on steeply dipping faults in the accretionary prism (Fukao 1979), slumping of sediments near the trench (Ma et al. 1991), and rupture reaching the ocean floor in non-accreting margins where the sediments are subducted along plate interface (Kanamori and Kikuchi 1993). We note that all of these mechanisms involve shallow and possibly slow sources (Polet and Kanmori 2000). Tsunami earthquakes are characterized by large $(M_s - M_w)$ and $(m_b - M_w)$ disparity (Kanamori and Kikuchi 1993) and anomalously low value of E_s/M_0 (Newman and Okal 1998; Ammon et al. 2006), where m_b is the short-period body-wave magnitude, E_s is the radiated seismic energy, and M_0 is the seismic moment. Based on these parameters and present state of technology, a rapid detection of a tsunami earthquake is now possible. However, tsunamis are often caused by events that do not qualify as tsunami earthquakes. Although the great earthquakes of 1952 Kamachatka, 1957 Aleutians, 1960 Chile, 1964 Alaska, and 2004 Sumatra produced the five largest tsunamis of the last 100 years, none of these events

qualify as tsunami earthquake. Because of their magnitude and location, such earthquakes should automatically give rise to early tsunami warning. It remains a challenge to assess tsunamigenic potential of events that do not fall in the category of tsunami earthquake but may generate large tsunamis. For example, the Nias earthquake of March 28, 2005 (M_w 8.6), generated smaller tsunami in relation to its magnitude (Geist et al. 2006). What parameter, based on seismic data, could have been used to rapidly detect this?

The *W*-phase CMT solution for earthquakes in the Sumatra–Andaman region is now available in less than 20 min, giving centroid location, M_w, and focal mechanism. These are critical elements toward early tsunami warning. Such a warning would be useful for the east coast of India and Sri Lanka, although not for the near-source region. We expect high tsunami potential from shallow and slow earthquakes. While the *W*-phase CMT solution yields the centroid depth, it does not provide any information on the details of the source, for example, possible slow slip on the fault. It follows that a parameter that is sensitive to both the depth and the source characteristics and may be estimated rapidly will be useful in estimating tsunami potential.

Shapiro et al. (1998), Iglesias et al. (2003), and Singh et al. (2008) reported that the ratio of total to high-frequency energy, E_r, is a useful parameter in depth discrimination. These studies show that E_r of earthquakes along the Pacific coast of Mexico, recorded on a broadband seismograph in Mexico City ($3° \leq \Delta \leq 5°$), is sensitive to the depth of the event: Shallower, near-trench events have larger E_r than the deeper ones. This suggests that earthquakes with large E_r may have high tsunamigenic potential. The dependence of E_r on depth arises from the fact that seismograms of shallower events at regional distance are enhanced at longer periods as compared to those of the deeper ones. The method is reminiscent of the work of Tsai and Aki (1970), which showed that surface-wave amplitude spectra could be used to determine focal depth. In fact, E_r includes both the effect of the depth and the source characteristics. In this sense, E_r provides useful complementary information to the centroid depth. In a somewhat similar approach, the energy content in the seismogram estimated from wavelet analysis has been proposed as a diagnostic tool for early tsunami by Chamoli et al. (2010).

Since E_r is a ratio, the effect of focal mechanism is canceled out. If path and distance from different events to a given station are roughly the same (thus requiring only a minor correction to normalize the data to a common distance), then it should be possible to compare E_r values of different earthquakes in a meaningful fashion. In this paper, we explore whether E_r, defined here as the ratio of broadband energy (0.01–2 Hz) to high-frequency energy (0.3–2 Hz), is a useful parameter for assessing tsunami potential. We compute E_r from broadband seismograms of earthquakes in the Sumatra–Andaman region recorded at VISK, a station on the east coast of India ($\Delta \sim 15$–$25°$). We also investigate whether the radiated seismic energy, E_s, of great earthquakes in the region, and hence E_s/M_0, can be estimated rapidly from broadband seismograms recorded at Indian stations using empirical Green's function technique.

2 Data

We searched for events in the Sumatra–Andaman region recorded at VISK since 1997, the year the station became operational. The selected events, with good signal-to-noise ratio, consist of earthquake of November 2, 2002 (M_w 7.2), the two great earthquakes (December 26, 2004, $M_w \sim 9.2$; March 28, 2005, M_w 8.6) and 41 of their aftershocks (which occurred before August 12, 2006), north Sumatra earthquake of April 6, 2010 (M_w 7.8), and Nicobar

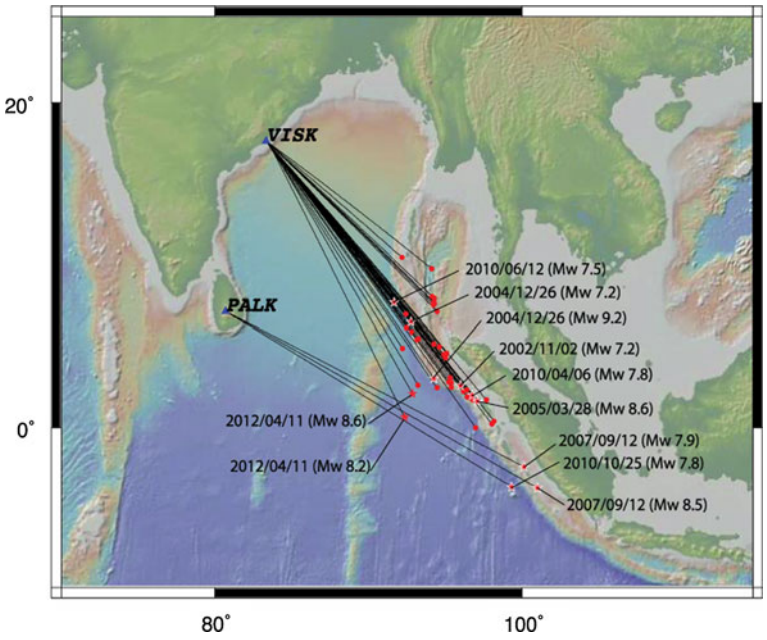

Fig. 1 Map showing stations VISK and PALK and epicenters of earthquakes (dot: $M_w < 7$; star: $M_w \geq 7$). Seismograms at VISK and PALK are used to analyze earthquakes in the Sumatra–Andaman and southern Sumatra regions, respectively. The date and magnitude of large earthquakes ($M_w \geq 7$) are given in the figure

earthquake of June 12, 2010 (M_w 7.5) (Fig. 1). The aftershocks of the two great earthquakes that were visibly contaminated by other events were excluded from the analysis.

In the analysis, we also included the two recent, great strike-slip earthquakes of north Sumatra (2012, M_w 8.6, 8.2) and south Sumatra earthquakes of September 12, 2007 (M_w 8.5, M_w 7.9), and October 25, 2010 (M_w 7.8). The events are listed in Table 1. The table includes the centroid depths reported in Global CMT catalog. Depth, H, if reported by Engdahl et al. (2007) is also given in the table. In our analysis, H is taken from Engdahl et al. for $M_w < 7$ if available; otherwise, we use the centroid depth. For larger earthquakes ($M_w \geq 7$), we use the centroid depth. The epicentral distance of the events in the Sumatra–Andaman and north Sumatra regions from VISK ranges between 1,234 and 2,515 km, M_w ranges between 5.5 and 9.2, and the depth ranges between 10 and 58 km (Table 1). The three south Sumatra earthquakes are located between 2,893 and 3,066 km from VISK. These distances are greater than for the other earthquakes listed in Table 1. For this reason, for the south Sumatra earthquakes, we used data from PALK, which is located at distance between 2,398 and 2,564 km.

3 Validation of the method and computation of E_r

We compute E_r from:

$$E_r = \frac{\int_{f_1}^{f_3} V^2(f)df}{\int_{f_2}^{f_3} V^2(f)df} \quad (1)$$

where $V^2(f) = V_N^2(f) + V_E^2(f) + V_Z^2(f)$ and V_i (f) is the Fourier velocity spectrum of i-th component, normalized to a common distance. The normalization distance was taken as

Table 1 Earthquakes from Sumatra–Andaman and southern Sumatra regions analyzed in this study

Date Year/M/Day	Time Hr:Min	Lat	Long	H, km[a]	Magnitude[c]	Mechanism φ δ λ	Station	R, km	E_r
2002/11/02	01:26	2.65	95.99	23/NA	7.2/7.6	297 16 73	VISK	2,165	8.0e2
2004/12/26	01:01	3.09	94.26	29/30	9.2/8.8	329 8 110	VISK	2,006	5.0e2
2004/12/26	04:21	6.61	92.79	14/15	7.2/7.5	351 27 121	VISK	1,601	1.9e4
2004/12/31	02:24	7.10	92.43	12/12	6.1	319 14 75	VISK	1,534	1.1e3
2004/12/31	12:05	6.03	92.80	12/17	6.0	359 39 143	VISK	1,651	7.5e1
2004/12/31	17:48	4.68	95.09	24/50	5.9	326 3 100	VISK	1,928	2.0e0
2005/01/01	01:55	2.55	95.38	26/26	5.6	305 21 80	VISK	2,130	1.8e1
2005/01/01	06:25	4.99	92.20	12/17	6.6	111 80–177	VISK	1,706	2.6e1
2005/01/01[d]	19:08	7.27	94.47	34/25	6.1	156 86–178	VISK	1,838	8.1e1
2005/01/02	08:27	3.16	95.30	12/16	5.7	285 50 81	VISK	2,072	2.1e1
2005/01/02[b]	15:36	6.25	92.47	12/25	6.3	340 28 89	VISK	1,610	5.2e1
2005/01/04	09:13	10.62	92.17	22/25	6.1	353 12 96	VISK	1,234	1.1e1
2005/01/06	00:56	5.07	94.62	51/58	5.7	333 27 110	VISK	1,861	2.0e0
2005/01/09	22:13	4.61	94.89	53/57	6.0	319 25 100	VISK	1,919	2.0e0
2005/01/26	17:30	8.18	94.15	12/19	5.5	165 72–162	VISK	1,576	1.2e1
2005/01/26[d]	22:00	2.51	94.44	12/16	5.9	306 31 78	VISK	2,073	1.7e2
2005/01/27	16:58	7.79	94.28	13/22	5.7	237 82 4	VISK	1,616	1.3e2
2005/01/27	18:52	7.83	94.26	15/10	5.5	144 80–178	VISK	1,611	1.1e2
2005/01/28	07:49	7.85	94.20	12/18	5.5	141 70–176	VISK	1,605	6.2e1
2005/02/02	01:30	9.93	94.10	12/25	5.5	247 58–62	VISK	1,447	2.4e1
2005/02/03	04:51	5.59	93.27	39/40	5.5	286 86 162	VISK	1,722	1.0e0
2005/02/05	17:35	8.07	94.27	12/10	5.9	91 80 5	VISK	1,594	1.1e2
2005/02/09[d]	13:27	4.48	94.97	50/53	6.0	316 24 95	VISK	1,936	6.0e0
2005/02/17	05:31	4.40	95.01	51/54	5.6	307 28 88	VISK	1,945	2.0e0
2005/02/18	19:33	5.26	94.25	44/45	5.6	327 28 106	VISK	1,818	3.0e0
2005/02/25	13:31	7.67	94.24	12/21	5.6	240 89 14	VISK	1,622	3.3e1
2005/02/26	12:56	2.84	95.38	12/23	6.7	297 6 72	VISK	2,105	2.5e2
2005/03/28	16:10	1.67	97.07	26/30	8.6/8.4	333 8 118	VISK	2,320	4.8e3
2005/03/29	05:16	2.30	96.3	40/40	5.9	309 24 108	VISK	2,216	1.1e1
2005/03/30[b]	16:19	2.87	95.24	12/25	6.4	305 7 82	VISK	2,094	7.4e1
2005/04/03	00:59	0.23	98.04	37/38	6.0	330 19 112	VISK	2,515	6.0e0
2005/04/03	03:11	1.75	97.67	49/50	6.3	326 23 110	VISK	2,360	8.0e0
2005/04/11	06:11	1.95	96.42	27/29	6.1	314 14 89	VISK	2,254	2.5e1
2005/04/28[b]	14:07	1.91	96.49	17/31	6.3	310 10 86	VISK	2,262	2.6e1
2005/05/14	05:05	0.42	98.18	41/40	6.7	327 20 90	VISK	2,509	3.2e1
2005/05/18	11.37	5.53	93.17	38/35	6.1	281 83 153	VISK	1,720	2.0e0
2005/05/19	01:55	2.00	96.74	12/25	6.9	297 7 75	VISK	2,272	9.3e1
2005/05/21	23:01	5.10	94.60	52/45	5.6	334 28 110	VISK	1,857	2.0e0
2005/11/19[b]	14:10	2.04	96.55	12/NA	6.4	311 9 85	VISK	2,255	5.6e1
2006/04/19	20:36	2.70	93.22	17/NA	6.2	111 66–176	VISK	1,980	5.1e1
2006/04/25	18:26	1.78	96.77	12/NA	6.3	293 7 66	VISK	2,294	2.4e2

Table 1 continued

Date Year/M/Day	Time Hr:Min	Lat	Long	H, km[a]	Magnitude[c]	Mechanism $\varphi\ \delta\ \lambda$	Station	R, km	E_r
2006/05/16	15:28	0.01	96.98	14/NA	6.8	358 82–31	VISK	2,462	2.8e2
2006/08/11	20:54	2.31	96.17	21/NA	6.2	310 9 88	VISK	2,206	2.6e2
2007/09/12	11:11	−3.78	100.99	24/NA	8.5/8.5	328 9 114	PALK	2,564	1.5e5
2007/09/12	23:49	−2.46	100.13	43/NA	7.9/8.1	317 19 102	PALK	2,415	1.7e4
2010/04/06	22:15	2.07	96.74	18/NA	7.8/7.9	307 7 88	VISK	2,266	2.9e3
2010/06/12	19:27	7.85	91.65	33/NA	7.5/7.5	220 66 32	VISK	1,416	2.9e2
2010/10/25	14:43	−3.71	99.32	12/NA	7.8/7.8	316 8 96	PALK	2,398	5.0e4
2012/04/11	08:39	2.24	92.78	40/NA	8.6	20 64 1	VISK	2,000	2.8e3
2012/04/11	10:43	0.76	92.25	54/NA	8.2	16 74–10	VISK	2,114	2.1e3

[a] First and second numbers refer to depths reported in Gobal CMT catalog and Engdahl et al. (2007), respectively

[b] Events chosen for the estimation of Q (see Appendix A) [c] First and second numbers refer to magnitudes M_w and M_s, respectively. If $M_w < 7$, then only M_w is listed

[d] Events whose spectra are compared in Fig. 2

2,000 km, which is roughly the distance of VISK from the hypocenters of the great 2004 earthquake and many of its aftershocks. The procedure of normalization is described in Appendix A. The time window used in the analysis began with the arrival of S wave and had a duration of ~1,500 s. (Test shows that ~900 s of signal may suffice.) The signals were Fourier-transformed, smoothed with a 1/6 octave-band filter, and 5 % tapered.

The upper limit of the integration in Eq. 1, f_3, was taken as 2 Hz. This ensured that the spectra were above the noise at the high-frequency end for all events considered in this study. Our choice of $f_3 = 2$ Hz was also guided by the fact that the normalization to a common distance leads to greater uncertainty at high frequencies. The lower limit of integration in the numerator, f_1, was taken as 0.01 Hz. This is the smallest frequency above which the spectra of all events were above noise. We set the lower limit in the denominator (f_2) as 0.3 Hz. Thus, in Eq. 1, the numerator and the denominator are proportional to broadband and high-frequency energy, respectively.

Figure 2 shows broadband seismograms of three aftershocks ($M_w \sim 6$) of the great Sumatra 2004 earthquake recorded at VISK at a distance of ~2,000 km. The depths of the events are 16 km, 25 km, and 53 km. The velocity spectra of these events are shown in Fig. 3. As these two figures illustrate, the shallow earthquake is enriched at long periods as compared to the deeper events. The spectra suggest that, for earthquakes of same M_w, the ratio of broadband to high-frequency energy, E_r, will be greater for the shallower event as compared to the deeper one.

4 Dependence of E_r on M_w

We expect the computed E_r to be a function of depth. However, since source spectrum depends on the size of the earthquake while the limits of integration in Eq. 1 are fixed for all events, E_r will also be a function of M_w. To correctly interpret the results, it is useful to establish the theoretical dependence on E_r on M_w. For this purpose, we computed E_r

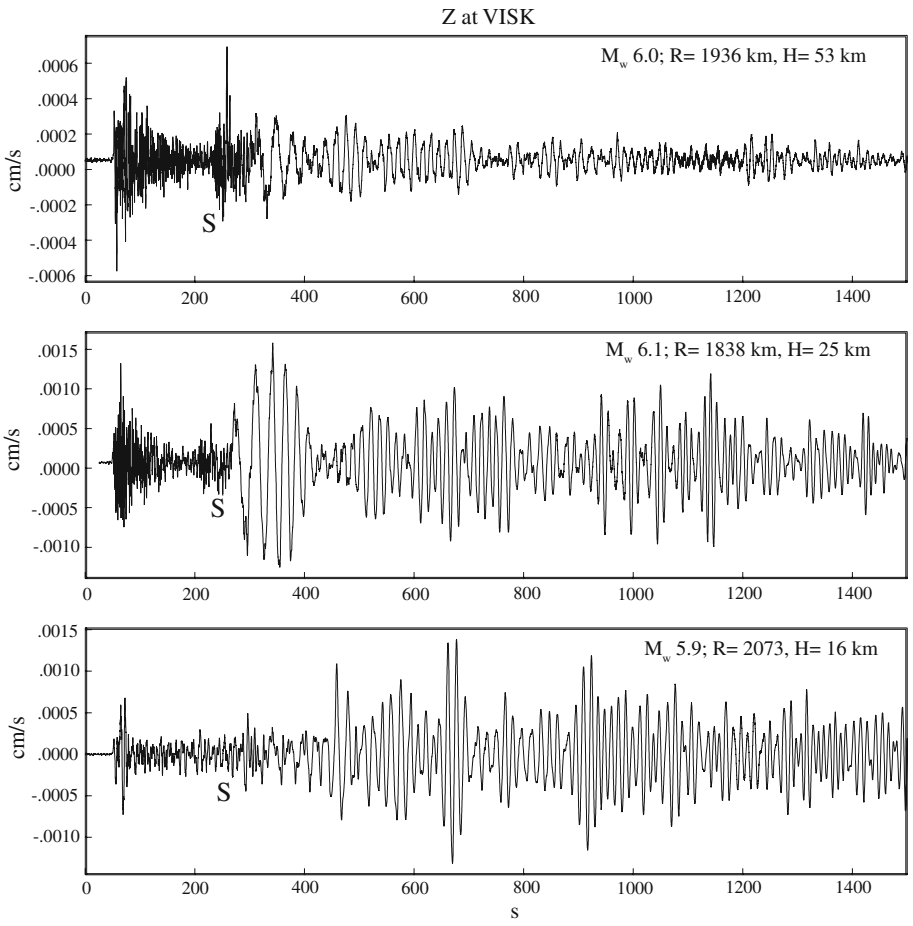

Fig. 2 Seismograms at VISK (Z component) of three earthquakes from Sumatra–Andaman region of about the same magnitude ($M_w \sim 6$) but different depth. The epicentral distance of these events is nearly equal. Note the relative enrichment of high-frequency signal of deeper events (*top* and *middle traces*) as compared to the shallow event (*bottom trace*). S-wave arrival is marked by letter *S*

assuming an ω^2 source model. In this case, *V(f)* in Eq. 1 is proportional to $f\dot{M}_0(f)e^{-\pi fR/UQ}$, where $\dot{M}_0(f) = M_0 f^2/\left(f^2 + f_c^2\right)$is the moment rate spectrum, f_c is the corner frequency, U is the group velocity (assumed here as 3.5 km/s), R is the hypocentral distance, and Q is the quality factor (Appendix A). In computing E_r, we assumed the Brune source model (Brune 1970) and a constant stress drop ($\Delta\sigma$) of 10 MPa.

4.1 E_r versus M_w

Figure 4 shows E_r versus M_w plot for earthquakes in the Sumatra–Andaman region. In the figure, events with depth $H < 25$ km, $25 \leq H < 40$ km, and $H \geq 40$ km are marked by circles, dots enclosed by circles, and dots, respectively. In most cases, for the same M_w, the shallower events have higher E_r values than the deeper ones. Although the depth range of the events varies by a factor of about 6 (10–58 km; Table 1), E_r for the same M_w varies by

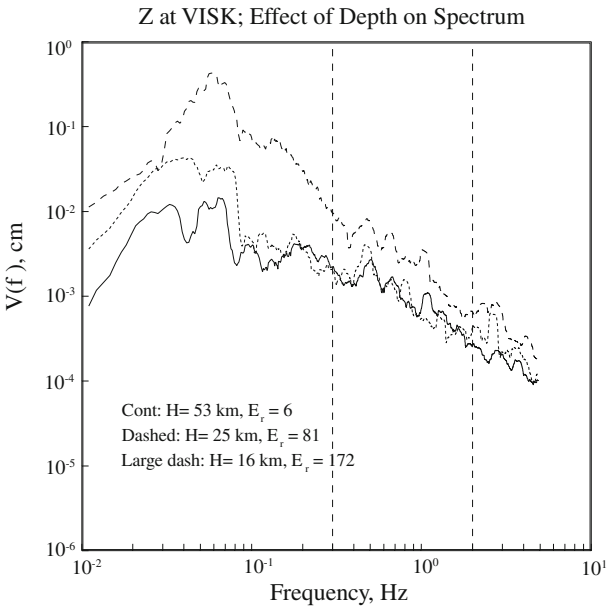

Fig. 3 Velocity spectra of the earthquakes shown in Fig. 2. Time window taken in the computation of the spectra is ~1,500-s long. Spectrum of shallow earthquake is enriched at long periods as compared to the deeper events. This suggest that, for earthquakes of same M_w, the ratio of broadband to high-frequency energy, E_r, will be greater for the shallower event as compared to the deeper one. Computed E_r values are 172, 81, and 6 for events of depths 16, 25, and 53 km, respectively (Table 1)

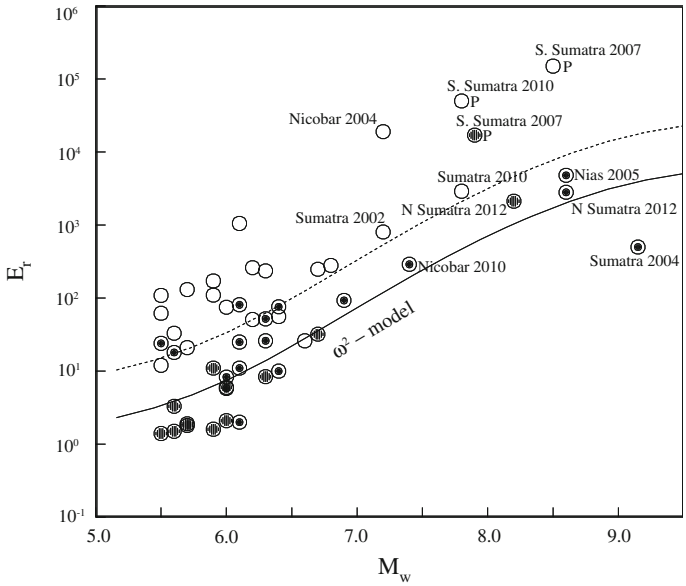

Fig. 4 E_r versus M_w for earthquakes of Sumatra–Andaman region. E_r of these events is computed from seismograms at VISK. E_r of three large/great earthquakes from southern Sumatra region, computed from data at PALK, is also shown. Circle: $H < 25$ km; dot with circle: $25 \leq H < 40$ km; dot: $H \geq 40$ km. For $M_w < 7.0$, H is taken from Engdahl et al. (2007) if available; otherwise, it is from Global CMT catalog (Table 1). For $M_w \geq 7.0$, H is the centroid depth. These events are identified in the figure. P: PALK. In general, E_r decreases with increasing depth. The continuous reference curve, based on ω^2 source model, divides the events with $H < 40$ km from deeper events. The *dashed reference curve*, whose ordinates are 4.5 times greater than that of the *continuous reference curve*, divides $H < 25$ km events from deeper ones

a factor of more than 100. Larger E_r for shallower earthquakes may be attributed to more efficient excitation of long-period surface-waves and possible slower nature of the shallower sources. Figure 4 also shows theoretically expected E_r versus M_w curve based on the ω^2 Brune source model with constant stress drop (10 MPa) (continuous curve). For convenience, we also show a dashed curve whose ordinate is shifted 4.5 times with respect to the continuous curve. Henceforth, we will call these two curves the reference curves. Increase in E_r with M_w, seen in the data, is in accordance with the shape of the reference curves. In general, the dashed and continuous reference curves separate events with depth $H < 25$ km, $25 \leq H < 40$ km, and $H \geq 40$ km events fairly well. Figure 4 is encouraging: An earthquake in the Sumatra–Andaman region for which E_r at VISK falls above the dashed reference curve is very likely to be shallow in depth.

We note the following points in relation to earthquakes with $M_w \geq 7$ (Fig. 4):

(1) E_r of earthquakes of Sumatra in 2002 (M_w 7.2) and Nicobar in 2004 (M_w 7.2) and 2005 (M_w 7.2) are above the dashed reference curve. The centroid depths of these earthquakes are also less than 25 km. It is not known whether these earthquakes generated appreciable tsunami.

(2) E_r at VISK for the 2005 Nias earthquake (M_w 8.6) is slightly below the dashed reference curve. This is not surprising. It has been suggested that the tsunami generation during this event was deficient in relation to its magnitude (e.g., Geist et al. 2006). A likely explanation for the relatively small E_r value and deficient tsunami generation is offered by the concentration of slip in the downdip part of the rupture area (Ammon et al. 2005; Ji 2005; Geist et al. 2006).

(3) E_r at VISK of the northern Sumatra earthquake of April 6, 2010 (M_w 7.8), is slightly above the dashed curve indicating shallow source. This agrees with the Global CMT depth of 20 km. E_r and M_w values of this earthquake suggest a tsunamigenic earthquake. However, the water depth at the epicenter is only 19 m. Based on the shallow water depth and pre-run model scenarios, INCOIS correctly issued a bulletin within about 37 min of the origin time, stating that there was no tsunami threat to India. The event demonstrates why availability of several key parameters is useful in correctly assessing tsunami potential of an earthquake.

(4) For the Nicobar earthquake of 2010 (M_w 7.4), E_r at VISK points to a source depth between 25 and 40 km. This is in agreement with the Global CMT depth of 37 km, suggesting a non-tsunamigenic earthquake. INCOIS, initially, issued a tsunami watch report, which was canceled about 1 h 32 min after the origin time of the earthquake, as the tide gauge at Andaman did not show any significant change.

(5) E_r values of the three southern Sumatra earthquakes are also plotted in Fig. 4. Since these have been computed from PALK recordings, these values are not directly comparable with the others in the figure. It is reassuring, however, that E_r of the shallower earthquakes of September 12, 2007, 11:11 (M_w 8.5, $H = 25$ km) and October 25, 2010 (M_w 7.9, $H = 12$ km), are higher with respect to the dashed reference curve than that of the deeper earthquake of September 12, 2007, 23:49 (M_w 7.9, $H = 43$ km). The tsunami caused by the earthquake of 2010 killed about 500 persons in Pagai Island. Tsunami alert was issued by the Pacific Tsunami Warning Centre and Indian authorities following the 2007, M_w 8.5 earthquake. A 1-m-high tsunami was recorded at Padang Island.

(6) E_r at VISK for the great 2004 Sumatra earthquake (M_w 9.2) is well below the continuous reference curve. This is intriguing. Why is E_r so low for this great earthquake, which generated such large tsunami and caused unprecedented loss? Below we address this issue.

(7) E_r values at VISK of the two recent, great, and extremely unusual strike-slip earthquakes offshore north Sumatra (2012, M_w 8.6, 8.2) fall between dashed and continuous curves, suggesting that the depth of significant slip was located between 25 and 40 km. Thus, the strike-slip focal mechanisms reported in the *W*-phase CMT solution and the low E_r values would have indicated a low tsunamigenic potential for both of these events. The centroid depths of the two events, as reported in the GCMT catalog, are 40 and 54 km, respectively (Table 1); the corresponding CMT depths given by U.S. Geological Survey are 40 and 43 km. These depths are somewhat greater than those inferred from the E_r values (between 25 and 40 km). We note that the centroid depths, reported by National Earthquake Information Center, U.S. Geological Survey, from the *W*-phase inversion are 25 and 16 km. Thus, the depth of significant slip during these earthquakes is, as yet, uncertain. Based on magnitude and location of the first great earthquake and pre-run modeling, INCOIS declared several zones to be potentially under tsunami threat. Only minor tsunamis were observed at several locations.

4.2 Low E_r for the great Sumatra earthquake (M_w 9.2)

An inspection of VISK recordings provides one possible cause of the relatively low value of E_r. Velocity and acceleration traces at VISK of the Sumatra (M_w 9.2) and the Nias earthquake (M_w 8.6) (Z component) are shown in Fig. 5. Various studies demonstrate that the rupture during the Sumatra earthquake lasted $\sim$600 s (e.g., Ni et al. 2005; Ishii et al. 2005; Ammon et al. 2005; de Groot-Hedlin 2005). As a consequence, high-frequency P waves overlap with S waves and the beginning of surface waves. This is clearly seen from a comparison of acceleration and velocity traces of the event (Fig. 5). For the Nias earthquake, the S waves are well separated from the P waves and their coda. The velocity Fourier spectra of these two events are shown in Fig. 6. As the time window used in the analysis begins at the arrival of S waves, the signal of the Sumatra earthquake includes high-frequency P waves. It gives rise to slow spectral falloff at $f \geq 0.2$ Hz, and the corresponding increase in high-frequency energy results in small value of E_r (Eq. 1). Small value of E_r for this great earthquake, however, does not argue against E_r being a useful parameter for early tsunami warning, because, first, such long-duration, great-magnitude event is infrequent and, second, such great-magnitude earthquake and its location merit early tsunami warning irrespective of the E_r value.

5 Rapid estimation of radiated energy, E_s, of great earthquakes

As mentioned above, tsunami earthquakes are characterized by an anomalously low value of E_s/M_0 (e.g., Newman and Okal 1998; Venkataraman and Kanamori 2004; Ammon et al. 2006), where E_s is the radiated seismic energy. Here, we test whether rapid and reliable estimation of E_s, hence of E_s/M_0, of earthquakes in Sumatra–Andaman region is possible in an operational mode using broadband seismograms from India. We note that the stations of India lie within the distance range about 15°–25° from Sumatra–Andaman earthquakes. For this reason, methods based on teleseismic P-wave group (e.g., Boatwright and Choy 1986) may not be suitable for the estimation of E_s.

An alternative is to use the empirical Green's function (EGF) technique (e.g., Venkataraman et al. 2002; Singh et al. 2004). Recordings of a smaller earthquake from the same

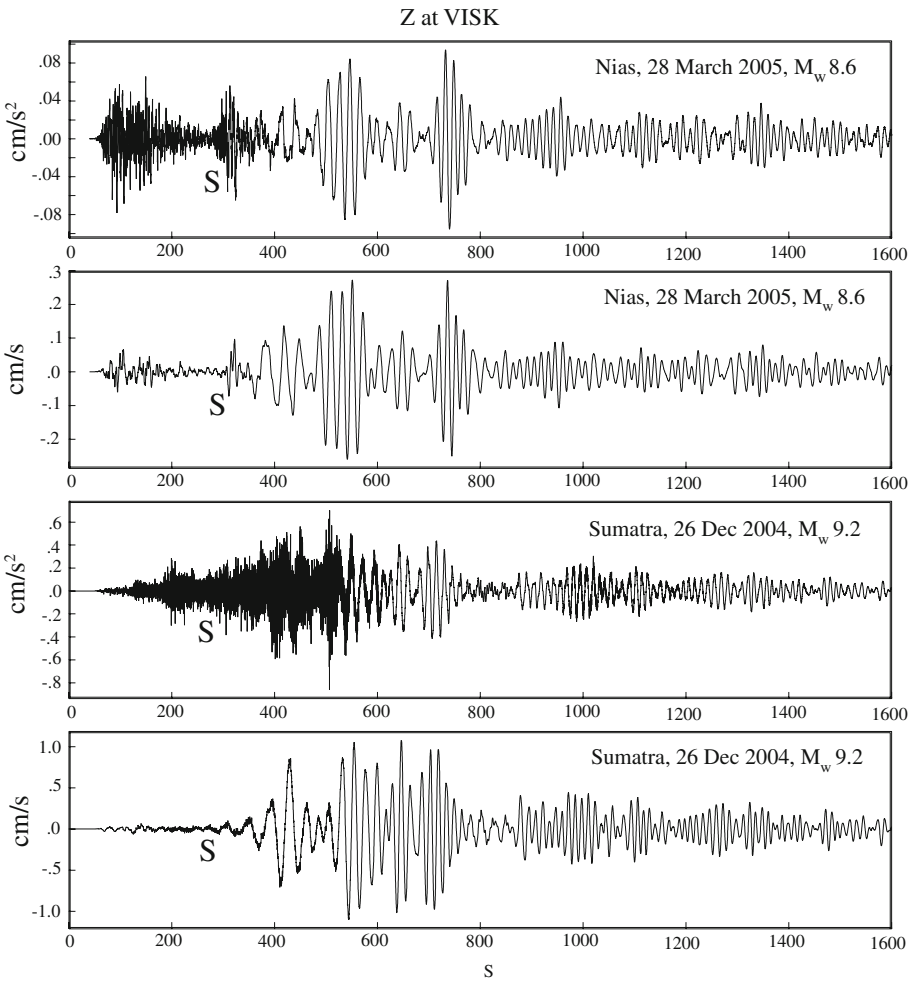

Fig. 5 Velocity and acceleration traces (Z component) of December 26, 2004 (M_w 9.2), and March 28, 2005 (M_w 8.6), earthquakes recorded at VISK. S-wave arrival is marked by letter *S*

region can be used as EGF provided that the location and focal mechanism of the EGF and the larger, target event are similar. The method has the advantage that it does not require corrections for attenuation and local site effects. The magnitude of the target event, however, should be at least two units greater than that of the EGF. Assuming point-source, far-field approximation to be valid, E_s can be written as (Vassiliou and Kanamori 1982):

$$E_s = \frac{4\pi}{5\rho\beta^5}\int_0^\infty f^2\dot{M}^2(f)df \tag{2}$$

where $\dot{M}_0(f)$ is the moment rate spectrum, and ρ is the density, and β is the shear-wave velocity in the source region. Let us assume that the seismogram of an appropriate smaller-magnitude earthquake is available such that it can be used as an EGF for the mainshock.

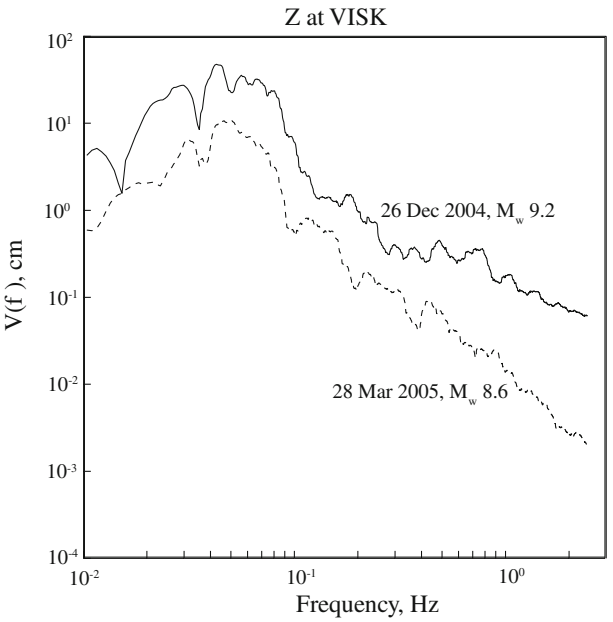

Fig. 6 Fourier velocity spectra of December 26, 2004 (M_w 9.2), and March 28, 2005 (M_w 8.6), earthquakes recorded at VISK. The time window used in the computation of spectra begins with the arrival of S wave and is ~1,500 s long

The moment rate spectrum of the mainshock can then be approximated from the ratio of the spectrum of the mainshock to the EGF and multiplying the ratio by M_o of the EGF event. This approximation is valid at frequencies smaller than the corner frequency of the EGF. Earthquakes with $M_w \geq 6.0$ in Sumatra–Andaman region produce seismograms in India with acceptable signal-to-noise ratio in the frequency band of interest, so they are likely candidates to be used as EGF. For rapid estimation of *Es* using the EGF technique, we would like to set, a priori, the upper limit of integration, in Eq. 2, to a fixed value, say, f_u, which is smaller than the corner frequency of the EGF. For EGF and mainshock whose moment- magnitudes are ~6 and ≥ 8, respectively, a reasonable choice of f_u is 0.1 Hz. The contribution to E_s of frequencies greater than f_u, can be obtained by assuming an f^{-2} falloff of moment rate spectrum, $\dot{M}_0(f)$, beyond f_u. This contribution is given by $\left(4\pi/5\rho\beta^5\right) f_u^3 \dot{M}_0^2(f_u)$. In our case, we set the lower limit of integration, f_l, in Eq. 2 at 0.005 Hz. The signal is above noise at frequencies ≥0.005 Hz for the EGF events. We will assume that the corner frequency of the mainshock is greater than 0.005 Hz. In this case, the contribution to E_s from the frequency range 0–0.005 Hz is given by $\left(4\pi/5\rho\beta^5\right)\left(f_l^3/3\right)M_0^2$, where $f_l = 0.005$ Hz. This contribution to E_s is negligible as compared to that from $f > 0.005$ Hz.

The precise depth extent of the mainshock rupture will, of course, be unknown immediately after the earthquake. In computing E_s, we will take $\rho = 3.2$ gm/cm^3 and $\beta = 4.62$ km/s, appropriate for upper mantle structure. If the true values are ρ_t and β_t, then the computed E_s needs to be multiplied by a factor $(3.2/\rho_t)(4.62/\beta_t)^5$.

5.1 Sumatra earthquake of January 26, 2004

The point-source approximation is violated by the great Sumatra earthquake, whose rupture length was ~1,400 km (e.g., Ammon et al. 2005). We, nevertheless, assume that Eq. 2 can be used for rough estimation of E_s. We used aftershocks of January 2, 2005 (6.25°N, 92.47°E; M_w 6.4), and January 4, 2005 (10.62°N, 92.17°E; M_w 6.1), as EGFs (Table 1). Figure 7a shows $\dot{M}_0(f)$ of the Sumatra earthquake retrieved from the EGF technique (continuous curve). The figure includes $\dot{M}_0(f)$ reported by Stein and Okal (2005) at ultra-low frequencies and in Global Centroid Moment-Tensor (GCMT) catalog at about 0.0025 Hz. It also shows $\dot{M}_0(f)$ computed from the source time function of model III of Ammon et al. (2005). We note that $\dot{M}_0(f)$ from the EGF technique and from model III is fairly consistent in the frequency range of 0.005–0.1 Hz. We computed E_s in this frequency band using Eq. 2. The result is shown in Fig. 7b as a function of azimuth. For the entire

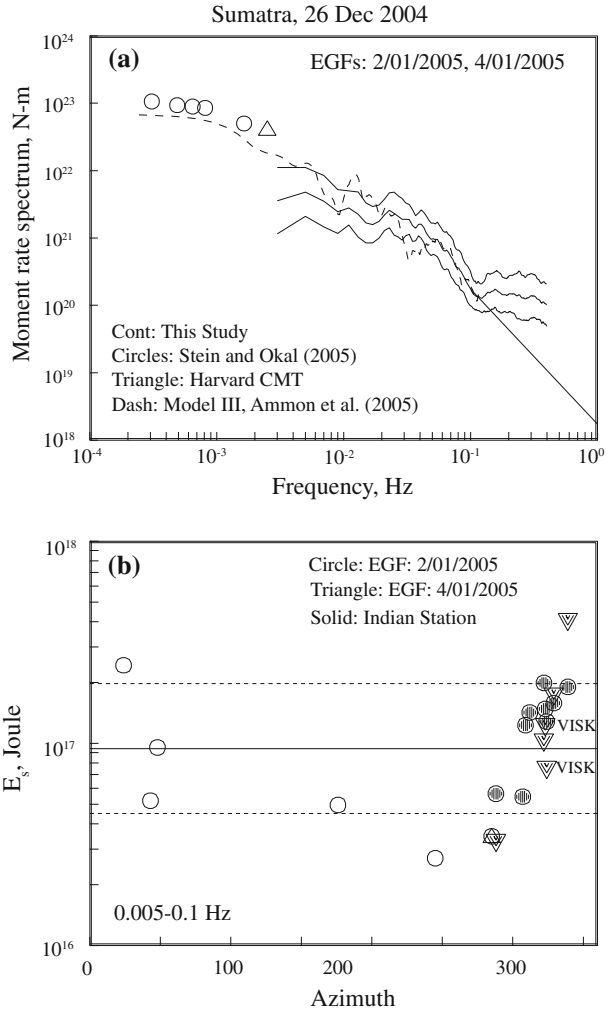

Fig. 7 **a** Median and ±1 standard deviation curve of moment rate spectrum, $\dot{M}_0(f)$, of the great 2004 Sumatra earthquake retrieved from the EGF technique (*continuous line*). *Circles*: $\dot{M}_0(f)$ reported by Stein and Okal (2005) at ultra-low frequencies. *Triangle*: M_o reported in Global Centroid Moment-Tensor (GCMT) catalog (*triangle*). $\dot{M}_0(f)$ computed from the source time function of model III of Ammon et al. (2005) is shown by *dashed line*. *Straight line* shows f^{-2} falloff of $\dot{M}_0(f)$ at $f > 0.1$ Hz. **b**. Radiated seismic energy, E_s, in the frequency band 0.005–0.1 Hz, plotted as a function of azimuth. *Solid symbols* show stations in India. *Horizontal lines* show median and ±1 standard deviation value of E_s

data set, log $E_s = 16.974 \pm 0.320$, which gives a median $E_s = 9.42 \times 10^{16}$ J. E_s in the frequency band 0–0.005 Hz is 7.0×10^{15} J. Median $\dot{M}_0(f_u)$ at $f_u = 0.1$ Hz is 1.74×10^{20} N-m (Fig. 7). This yields $E_s = 1.12 \times 10^{16}$ J for $f > 0.1$ Hz. Thus, our estimate of total E_s is 1.12×10^{17} J. We note that E_s estimated from the Indian stations (shown by solid symbols in Fig. 7), as well as from VISK alone, is close to this value. For comparison, Choy and Boatwright (2007) and Kanamori (2006) report $E_s = 1.4 \times 10^{17}$ J and 3.0×10^{17} J, respectively. These values are close to the one reported here. Our estimate of E_s differs from that by Kanamori (2006) mostly at $f > 0.1$ Hz: 1.11×10^{16} J versus 1.6×10^{17} J. We recall that our estimation of E_s in the frequency band 0.1–∞ Hz relies on the assumption of f^{-2} falloff of the moment rate spectrum, while Kanamori's (2006) estimate uses observed seismograms, and, hence, it may be more reliable.

From $E_s = 1.12 \times 10^{17}$ J and $M_0 = 1.2 \times 10^{23}$ N m, we obtain $E_s/M_0 = 1.0 \times 10^{-6}$. If we consider the range of the reported values of E_s ($1.12–3.0 \times 10^{17}$ J) and M_0 ($0.6–1.3 \times 10^{23}$ N m), then E_s/M_0 ranges between 1.1×10^{-6} and 5.0×10^{-6}. These

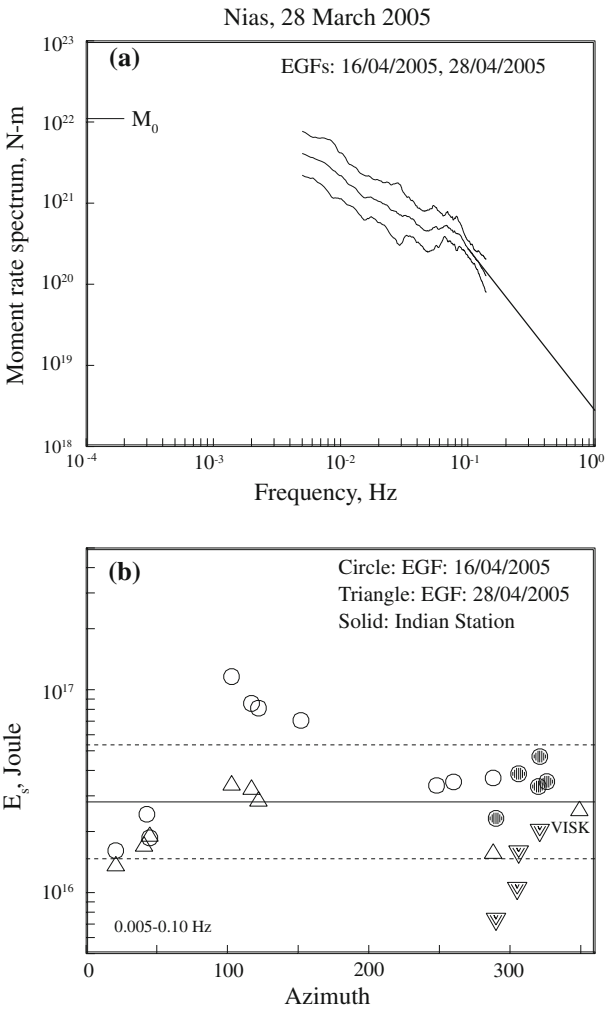

Fig. 8 **a** Median and ± 1 standard deviation curve of moment rate spectrum, $\dot{M}_0(f)$, of the great 2005 Nias earthquake retrieved from the EGF technique (*continuous line*). *Straight line* shows f^{-2} falloff of $\dot{M}_0(f)$ at $f > 0.1$ Hz. **b** Radiated seismic energy, E_s, in the frequency band 0.005–0.1 Hz, plotted as a function of azimuth. *Solid symbols* show stations in India. *Horizontal lines* show median and ±1 standard deviation value of E_s

values are only somewhat smaller than that of other large/great subduction zone earthquakes (Venkataraman and Kanamori 2004).

5.2 Nias earthquake of March 28, 2005

To estimate E_s of Nias earthquake of 2005 (M_w 8.6), we took aftershocks of April 16, 2005 (1.67°N, 97.46°E; M_w 6.4), and April 28, 2005 (1.91°N, 96.49°E; M_w 6.3), as the EGFs. Figure 8a shows $\dot{M}_0(f)$ of the earthquake retrieved from the EGF technique (continuous curve). Figure 8b shows E_s as a function of azimuth. For the entire data set, log $E_s = 16.447 \pm 0.281$, which gives median $E_s = 2.80 \times 10^{16}$ J. Median $\dot{M}_0(f_u)$ at $f_u = 0.1$ Hz is 2.77×10^{20} N-m (Fig. 8). This yields $E_s = 1.90 \times 10^{16}$ J for $f > 0.1$ Hz. Thus, the total E_s is 4.70×10^{16} J. Again, E_s estimated from the Indian stations (shown by solid symbols in Fig. 8) and from VISK alone is close to this value. For this earthquake, Kanamori (2006) and Choy and Boatwright (2007) report E_s of 7.5×10^{16} J and 6.7×10^{16} J, respectively. With $M_0 = 1.1 \times 10^{22}$ N m, E_s/M_0 values range between 4.3 and 6.8×10^{-6}.

We note that our estimated E_s for $f > 0.1$ Hz of this earthquake is greater than that of the great 2004 earthquake: 1.90×10^{16} J versus 1.11×10^{16} J. The reason is that the median $\dot{M}_0(f_u)$ at $f_u = 0.1$ Hz of the Nias earthquake (Fig. 8) is greater than that of the 2004 earthquake (Fig. 7). It is possible that our assumption of f^{-2} falloff at $f > 0.1$ Hz for both earthquakes is not true, and E_s for the great 2004 earthquake, in fact, was greater than for the Nias earthquake in this frequency band.

We have shown above that EGF technique can be used to obtain a reliable estimate of radiated energy of great earthquakes in Sumatra–Andaman region recorded at stations in India. Generally, EGFs of $M_w \geq 6.0$ are needed for adequate signal-to-noise ratio in the frequency band of interest. This constrains the magnitude of the target event to $M_w \geq 8.0$.

For rapid estimation of E_s of a great earthquake in the Sumatra–Andaman region using the EGF technique, it will be critical to store recordings of moderate earthquakes along with their locations, M_0, depths, corner frequencies, and focal mechanisms in computer archives so that one or more appropriate EGF can be immediately retrieved once location and centroid moment tensor of the target event is determined.

6 Discussion and conclusions

In this paper, we have explored the ratio of broadband (0.005–2 Hz) to high-frequency energy (0.3–2 Hz), E_r, computed from regional seismograms recorded at VISK, as an additional parameter to assess the depth and the source characteristics and, hence, tsunami potential of earthquakes in the Sumatra–Andaman region. VISK is located on the east coast of India. The result shows that for moderate earthquakes ($M_w < 7.0$), E_r is greater for the shallower ones than for the deeper ones. A reference curve based on ω^2 source model, shown by the dashed line in Fig. 4, separates shallower earthquakes ($H < 25$ km) from the deeper ones. Extrapolation of the trend of E_r data of moderate earthquakes suggests that large/great earthquakes with E_r values above the dashed reference curve may have shallow centroid depth. The converse would be true if E_r is below the curve. E_r values of large/great earthquakes at VISK from Sumatra–Andaman region are, indeed, above the dashed reference curve for centroid depths <25 km and below it for depths ≥25 km. We find that earthquakes whose E_r values fall below the dashed curve did not produce appreciable tsunami. Consider, for example, the 2005 Nias (M_w 8.6) earthquake. Relatively low E_r of

this earthquake at VISK is in agreement with the slip being concentrated on the downdip part of the rupture area (Ji 2005). This earthquake caused smaller local tsunami than expected for its magnitude (e.g., Geist et al. 2006). Low E_r value for the 2010 Nicobar (M_w 7.4) earthquake also agrees with the minor tsunami or lack of it for this event. Great magnitude (M_w 7.8) and E_r above the dashed curve for the Sumatra 2010 earthquake point to a tsunamigenic earthquake. In this case, shallow water depth above the source area was the reason why no appreciable tsunami was reported. Unexpectedly, E_r at VISK is low for the 2004 Sumatra–Andaman earthquake (M_w 9.2). In this case, the reason, at least partly, appears to be large rupture duration ($\sim$600 s). This causes high-frequency P waves to contaminate S and surface waves used in the computation of E_r, and give rise to a low E_r value. However, we are not discouraged by this failure: an M_w 9.2 earthquake, located near a trench, merits a tsunami alert irrespective of its E_r value. Low E_r values of the two recent, great, strike-slip earthquakes offshore north Sumatra (2012, M_w 8.6, 8.2) suggests low tsunamigenic potential. This is in agreement with the observed small tsunami, although the strike-slip fault mechanism, involving small vertical sea-floor displacement, must also have played a critical role. In summary, based on physical ground, it is reasonable to assign a higher tsunamigenic potential to earthquakes with values of E_r above the reference curve, even though the available data on tsunami in the region since 1997, when VISK became operational, are too limited to provide its confirmation.

Seeking confirmation of E_r as a useful parameter for assessing tsunami potential, we supplemented the Sumatra–Andaman data with those from three large/great earthquakes of the southern Sumatra region recorded at PALK. The difference in the path requires caution in comparing these data with those from VISK. These earthquakes, nevertheless, support the hypothesis that earthquakes with larger E_r values have greater tsunamigenic potential.

E_r bears similarity with the parameter (E_s/M_0). Abnormally high E_r and low (E_s/M_0) are both measures of relatively low excitation of high-frequency radiation. An advantage of E_r may be its higher sensitivity to depth and lower sensitivity to detailed source characteristics as compared to that of the parameter (E_s/M_0). A disadvantage of E_r is that data from other stations and regions cannot be directly compared with those from VISK.

We conclude that the estimation of E_r using data at VISK, along with the *W*-phase CMT solution, would be useful in assessing the tsunami potential of earthquakes in the Sumatra–Andaman region. Additionally, the parameter (E_s/M_0) of great earthquakes could be estimated using regional seismograms from India stations using empirical Green's function technique. These parameters, along with $(M_s - M_w)$ or $(m_b - M_w)$ disparity, should lead to a more robust early tsunami warning system for the region.

Acknowledgments We thank H. Kanamori, J. Boatwright, G. Choy, and M. Ortiz for fruitful discussions. Communications with K. Abe are gratefully acknowledged. The research was partly supported by DGAPA (UNAM) project IN114809, CONACYT project 82595, and Indo-Mexican Cooperation Program in Science and Technology sponsored by CONACyT, Mexico, and Department of Science and Technology, India.

Appendix A

Normalization of observed spectra to a common distance of 2,000 km

The epicentral distance from VISK to Sumatra–Andaman events, listed in Table 1, varies between 1,100 and 2,515 km (Table 1, Fig. 1). Before computing E_r, the observed spectra must be reduced to a common distance. This distance has been chosen as 2,000 km. To normalize the spectra, we assume that geometrical spreading and anelastic attenuation are

given by $R^{-1/2}$ (surface waves) and $e^{\frac{-\pi fR}{UQ(f)}}$, respectively, where R is the hypocentral distance, U is the group velocity (taken here as 3.5 km/s), f is the frequency, and $Q(f)$ is the quality factor. We selected four shallow events of nearly the same magnitude (M_w 6.3–6.4), located in the distance range of 1,610 and 2,262 km (Table 1). Global CMT depths of these events are 12 km. The depths of only three of these events have been determined by Engdahl et al. (2007). They lie between 25 and 31 km (Table 1). We assume that the source spectra of these events are the same. Figure 9 shows velocity spectra (Z component) of the four events. We attribute the difference in the spectra to geometrical spreading and anelastic attenuation. Under these assumptions, the spectral ratio of event i with respect to a reference event r at VISK may be written as:

$$[V_i(f)/V_r(f)] = (R_r/R_i)^{1/2} e^{-\pi f(Ri-Rr)/UQ(f)} \quad (3)$$

The earthquake closest to VISK (2005/01/02; 15:36; R = 1,610 km; Table 1) was taken as the reference event. We take logarithm of both sides of Eq. 3 and compute $Q^{-1}(f)$ at selected frequencies. $Q^{-1}(f)$ was computed for the geometrical mean of the spectral amplitudes of the two horizontal components and the vertical component separately.

Figure 10 shows $Q^{-1}(f)$ for each of the three events at discrete frequencies in the range 0.3–5 Hz, while Fig. 10 shows the mean value and ± 1 standard deviation of $Q^{-1}(f)$. The method leads to unreliable results at lower frequencies. $Q^{-1}(f)$ at these frequencies, shown in Fig. 10, were estimated by fixing its value as 0.0067 at 0.01 Hz (Ben-Menahem 1965) and smoothly interpolating it between 0.01 and 0.3 Hz. A choice of $Q^{-1}(f) = 0.001$ at 0.01 Hz (e.g., Cormier 1982) changes the estimate of E_r generally by less than 10 %. The mean values of $Q^{-1}(f)$, shown by dots in the figure, and geometrical spreading of $R^{-1/2}$ were used in normalizing observed spectra to a common distance of 2,000 km. Figure 9 shows the spectra of the four events (Z component) after this normalization. As expected, the spectra are reasonably similar. We note that the parameters used in normalization are

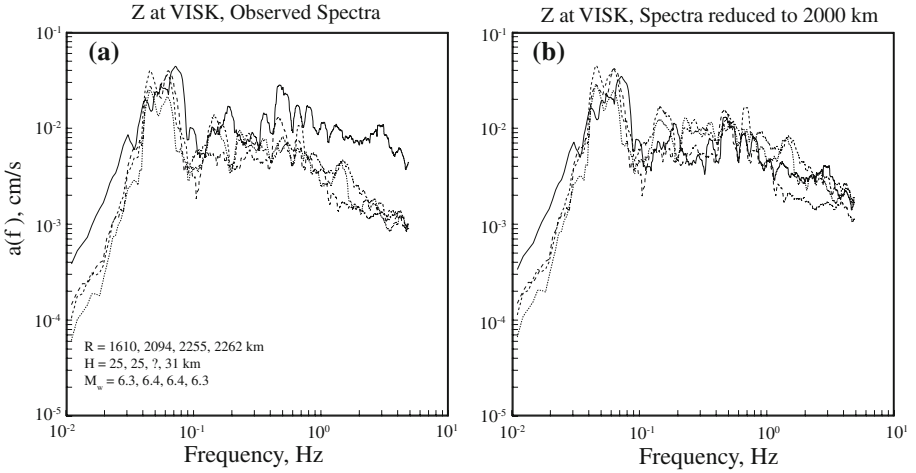

Fig. 9 **a** Fourier acceleration spectra (Z component) of four earthquakes from Sumatra–Andaman region recorded at VISK (Table 1). The earthquakes have similar magnitudes and depths, but their epicentral distance varies between 1,610 and 2,262 km. The depth of one of the events is not available in Engdahl et al. (2007). It is indicated by a *question mark*. **b** Fourier acceleration spectra of the four earthquakes normalized to a common distance of 2,000 km

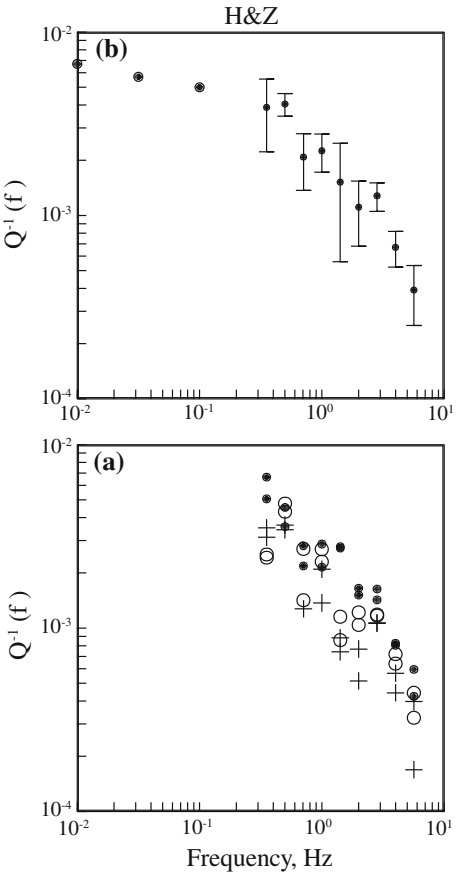

Fig. 10 $Q^{-1}(f)$ as a function of frequency. **a** $Q^{-1}(f)$ for each event at selected frequencies ($0.3 \leq f \leq 5$ Hz). Estimations from both horizontal and vertical components are included. **b** Mean and ± 1 standard deviation of $Q^{-1}(f)$. $Q^{-1}(f)$ at 0.01 Hz is taken as 0.0067 (see text) and smoothly interpolated between 0.01 and 0.3 Hz

the same for all trajectories. Since this may introduce large error, caution must be exercised in comparing E_r when the trajectories are very different.

References

Abe K (1979) Size of great earthquakes of 1837–1974 inferred from tsunami data. J Geophys Res 84:1561–1568

Ammon CJ, Ji C, Thio H-K, Robinson D, Ni S, Hjorleifsdottir V, Kanamori H, Lay T, Das S, Helmberger D, Ichinose G, Polet J, Wald D (2005) Rupture process of the 2004 Sumatra–Andaman earthquake. Science 308:1133–1139

Ammon CJ, Kanamori H, Lay T, Velasco AA (2006) The 17 July 2006 Java tsunami earthquake (M_w7.8). Geophys Res Lett 33:L24308. doi:10.10239/2006GLO26303

Ben-Menahem A (1965) Observed attenuation and Q values of seismic surface waves in upper mantle. J Geophys Res 70:4641–4651

Boatwright J, Choy GL (1986) Teleseismic estimates of the energy radiated by shallow earthquakes. J Geophys Res 91:2095–2112

Brune JN (1970) Tectonic stress and the spectra of seismic shear waves from earthquakes. J Geophys Res 75:4997–5009

Brune JN, Engen GR (1969) Excitation of mantle Rayleigh waves of period 100 seconds as a function of magnitude. Bull Seismol Soc Am 59:923–933

Chamoli A, Swaroopa Rani V, Srivastava K, Srinagesh D, Dimri VP (2010) Wavelet analysis of the seismograms for tsunami warning. Nonlin Process Geophys 17:569–574
Choy GL, Boatwright J (2007) The energy radiated by the 26 December 2004 Sumatra–Andaman earhtquke estimated from 10-minute P-wave windows. Bull Seismol Soc Am 97:S18–S24
Cormier VF (1982) The effect of attenuation on seismic body waves. Bull Seismol Soc Am 72:S169–S200
Dattatrayam RS, Bhatnagar AK, Suresh G, Baidya PR, Gautam JL (2009) Real time earthquake monitoring for early warning of tsunamis in Indian ocean region. Mausam, Diamond Jubilee Volume 253–264
de Groot-Hedlin CD (2005) Estimation of the rupture length and velocity of the great Sumatra earthquake of Dec 26, 2004 using hydroacoustic signals. Geophys Res Lett 32:L11303. doi:10.1029/2005GL022695
Engdahl ER, Villaseñor A, DeShon HR, Thurber CH (2007) Teleseismic relocation and assessment of seismicity (1918–2005) in the region of the 2004 Mw 9.0 Sumatra–Andaman and 2005 Mw 8.6 Nias Island great earthquakes. Bull Seismol Soc Am 97:S43–S61
Fukao Y (1979) Tsunami earthquake and subduction processes near deep sea trenches. J Geophys Res 84:2303–2314
Geist EL, Bilek SL, Arcas D, Titov VV (2006) Differences in tsunami generation between the December 26, 2004 and March 28, 2005 Sumatra earthquakes. Earth Planets Space 58:185–193
Hayes G, Rivera L, Kanamori H (2009) Source inversion of the W-phase: real-time implementation and extension to low magnitudes. Seism Res Lett 80:817–822
Iglesias A, Singh SK, Pacheco JF, Alcántara L, Ortiz M, Ordaz M (2003) Near trench Mexican earthquakes have anomalously low peak accelerations. Bull Seismol Soc Am 93:953–959
Ishii M, Shearer PM, Houston H, Vidale JE (2005) Extent, duration and speed of the 2004 Sumatra–Andaman earthquake imaged by the H-net array. Nature 435:933–936
Ji C (2005) Updated result of the 05/03/2005 (M_w8.5), Sumatra earthquake, http://www.gps.catech.edu/%Ejichen/Earthquake/2005/sumatra/sumatra.html
Kanamori H (1972) Mechanisms of tsunami earthquakes. Phys Earth Planet Inter 6:346–359
Kanamori H (1977) The energy release in great earthquakes. J Geophys Res 82:2981–2987
Kanamori H (2006) The radiated energy of the 2004 Sumatra–Andaman earthquake. In: Abercrombie R, McGarr A, Kanamori H, Di Toro G (eds) Earthquakes: radiated energy and the physics of faulting, Geophysical monograph series 170. American Geophysical Union, Washington, DC, pp 59–68
Kanamori H, Kikuchi M (1993) The 1992 Nicaragua earthquake: a slow tsunami earthquake associated with subducted sediments. Nature 361:714–716
Kanamori H, Rivera L (2008) Source inversion of W phase: speeding up seismic tsunami warning. Geophys J Int 175:222–238. doi:10.1111/j.1365-246X.2008.03887.x
Lockwood OG, Kanamori H (2006) Wavelet analysis of the seismograms of the 2004 Sumatra–Andaman earthquake and its application to tsunami early warning. Geochem Geophys Geosyst 7:Q09013. doi:10.1029/2006GC001272
Ma K-F, Satake K, Kanamori H (1991) The origin of the tsunami excited by the 1989 Loma Prieta earthquake-faulting or slumping. Geophys Res Lett 18:637–640
Newman AV, Okal EA (1998) Teleseismic estimates of radiated seismic energy: the E/M_0 discriminant for tsunami earthquakes. J Geophys Res 103:26885–26898
Ni S, Kanamori H, Helmberger D (2005) High-frequency radiation from the 2004 great Sumatra–Andaman earthquake. Nature 434:382
Polet J, Kanmori H (2000) Shallow subduction zone earthquakes and their tsunamigenic potential. Geophys J Int 142:684–702
Shapiro NM, Singh SK, Pacheco JF (1998) A fast and simple diagnostic method for identifying tsunamigenic earthquakes. Geophys Res Lett 25:3911–3914
Singh SK, Pacheco JF, Bansal BK, Pérez-Campos X, Bhattacharya SN, Dattatrayam RD, Suresh G (2004) A source study of Bhuj, India, earthquake of 26 January, 2001 ($M_w = 7.6$). Bull Seismol Soc Am 94:1195–1206
Singh SK, Pérez-Campos X, Iglesias A, Pacheco JF (2008) An exploratory study for rapid estimation of critical source parameters of great subduction-zone earthquakes in Mexico. Geofisica Internacional 47:355–369
Singh SK, Pérez-Campos X, Iglesias A, Melgar D (2012) A method for rapid estimation of moment magnitude for early tsunami warning based on coastal GPS networks. Seism Res Lett 83:516–530. doi:10.1785/gssrl.83.3.516
Stein S, Okal E (2005) Speed and size of the Sumatra earthquake. Nature 434:581–582
Talandier J, Okal EA (1989) An algorithm for automated tsunami warning in French Polinesia based on mantle magnitudes. Bull Seismol Soc Am 85:606–613
Tsai Y, Aki K (1970) Precise focal depth determination from amplitude spectra of surface waves. J Geophys Res 75:5729–5743

Vassiliou MS, Kanamori H (1982) The energy release in earthquakes. Bull Seismol Soc Am 72:371–387
Venkataraman A, Kanamori H (2004) Observational constraints on the fracture energy of subduction zone earthquakes. J Geophys Res 109:B05302. doi:10.1029/2003JB002549
Venkataraman A, Rivera L, Kanamori H (2002) Radiated energy from the 16 October 1999 Hector Mine earthquake: regional and teleseismic estimates. Bull Seismol Soc Am 92:1256–1265